Bull. Mater. Sci., Vol. 37, No. 6, October 2014, pp. 1411–1418. © Indian Academy of Sciences.

Formation and surface characterization of nanostructured Al_2O_3–TiO_2 coatings

VAIRAMUTHU RAJ* and MOHAMED SIRAJUDEEN MUMJITHA

Advanced Materials Research Laboratory, Department of Chemistry, Periyar University, Salem 636 011, India

MS received 20 December 2012; revised 6 March 2013

Abstract. One pot synthesis of Al_2O_3–TiO_2 nanoceramic coatings from environment-friendly potassium titanium oxalate (PTO) electrolyte using facile electrochemical anodization has been reported for the first time. Systematic analysis of the anodization parameters such as applied current density and concentration of the PTO electrolyte influence on the morphology of the ceramic coatings was done. The textural properties of the coatings (thickness, growth rate, coating ratio) showed a linear regime with current density and electrolyte concentration decreases up to a certain level and then decreases. The growth process, distribution of chemical elements, phase constitutions and corrosion resistance of the coatings were investigated by scanning electron microscopy (SEM), energy dispersive X-ray spectroscopy (EDX), X-ray diffraction (XRD), Tafel polarization technique and electrochemical impedance spectroscopy (EIS). The relation between the corrosion resistivity of the anodic coating and the aforementioned anodization parameters is investigated. The mechanisms that are involved in the formation of the ceramic coatings are also discussed. The coatings formed from 30 g/L concentration of PTO and 0·02 A/cm^2 current density show good morphology, textural properties and optimum corrosion resistance.

Keywords. Al_2O_3–TiO_2 nanoceramic coatings; formation mechanism; surface characteristics; corrosion studies.

1. Introduction

Aluminium and its alloys are important materials of research. This is because aluminium is abundant in nature, cost-effective, easy to handle and it is an important metal due to its high technological value, electrical capacity and wide range of industrial applications (Diggle *et al* 1969; Hoyer *et al* 1995; Hoyer *et al* 1996; Martin 1996; Despic *et al* 1998) especially in aerospace and household articles. When Al metal is exposed to the atmosphere, it undergoes a process of corrosion that leads to the build up of a thin layer on its surface of the oxides and hydroxides coming from the reaction of the metal itself with the aqueous vapour present in the air. These reaction products protect the surface from further alterations in some circumstances. Yet, the behaviour of the protective layers can be modified in order to meet some specific requirements or simply to lower the surface reactivity. Still, a low-cost fabrication of high-quality nanostructured coatings with controllable properties is a significant and ongoing challenge within nanoscience and nanotechnology. For minimizing the corrosion of Al metal, single oxide alumina nanocoatings have been reported previously (Deng *et al* 2003; Ren *et al* 2004; Patermarakis and Kytopoulos 2009; Zhao *et al* 2009). Despite wide applications, alumina nanocoatings have their own deficiencies and confines such as lower wear resistance, abrasion resistance and hardness. This triggered the need to find an alternative material to overcome these limitations. As a consequence, binary mixed oxides such as nanoceramics have been developed.

Al_2O_3–TiO_2 is one of the binary mixed oxides that offer an attractive combination of corrosion resistance, mechanical strength, interfacial adhesion and thermal property (Xue *et al* 2002; Wang *et al* 2004; Curran and Clyne 2005). Al_2O_3–TiO_2 material has been synthesized using ball milling (Takahashi *et al* 2002), spray drying (Liu *et al* 2005), sol–gel (Yuan *et al* 2004), hot pressing (García-Benjume *et al* 2009), plasma spraying (Wang *et al* 2009), wet chemical synthesis (Wunderlich *et al* 2004) and high-temperature oxidation (Ibrahim *et al* 1999). The transfer of this advantage to coatings becomes questionable due to the insufficient adhesion of the coatings to the base material. Most of the synthetic methods require a multistep process, high temperature and also the materials preparation is comparatively complex. So, one such technique with simple handling, high composite effectiveness and bright prospects for industrial application to produce ceramic coatings becomes a key technical issue. Among various synthesis methods, electrochemical anodization has demonstrated a facile and excellent approach to

*Author for correspondence (alaguraj2@rediffmail.com)

increase the life span of aluminium by fabricating ceramic coating on Al foil. Even though each synthetic method has its own unique advantages, anodization has become increasingly popular owing to the process flexibility and environment friendliness. It is superior to other techniques due to the following advantages such as low production cost, single-step process, simplicity of materials preparation and handling, as well as more control over the synthesis process. Anodization can increase the film thickness, hardness, corrosion resistance and wear resistance and provide better adhesion of the coatings to the bare metal.

The goal of this research was to construct alumina-titania coatings on Al foil by applying anodization technique using low-current density at room temperature, so that the production cost of such potentially important materials can be minimized. The consequences of different anodization parameters such as current density and concentration of the electrolyte on electrochemical corrosion behaviour, surface morphology, composition and mechanism of film growth of the alumina-titania nanoceramic coatings fabricated using PTO have been studied in order to maximize the achievement of these structures.

2. Experimental

A typical two-electrode electrochemical cell was used with the working electrode of Al foil having the working area of about 1 cm^2 and a counter electrode of lead sheet. Prior to anodization, the surface of the annealed samples of Al was degreased, alkali cleaned and desmutted for 1 min and weighed (W_1) (Wernick *et al* 1987; Raj and Mubarak Ali 2009). The anodization was carried out in various amounts of PTO (10–50 g/L) under various current densities (0·01–0·04 A/cm^2) for 45 min at room temperature. To maintain a uniform temperature and chemical distribution, the bath was stirred during anodization. After anodization, the specimens were weighed (W_2) and the anodic coating was stripped by a mixture of 0·4 M H_3PO_4 and 0·2 M CrO_3 for 15 min at 60 °C and weighed (W_3) to find out the exact amount of Al dissolved and coatings formed. The amorphous, as-anodized samples were crystallized by oxygen annealing at 500 °C for 5 h. The actual weight of the oxide coating was obtained from $W_2 - W_3$. The coating ratio (Wernick *et al* 1987; Mubarak Ali and Raj 2010) was obtained by the following formula

Coating ratio = weight of the coating ($W_2 - W_3$)/
weight of Al dissolved ($W_1 - W_3$).

The surface morphology, crystallographic characteristics and elemental composition of the nanoceramic coatings were observed by SEM, XRD and EDX, respectively. The ability of the ceramic coatings to shield the aluminium from corrosion in seawater was studied by potentiodynamic polarization and electrochemical impedance spectroscopy in 3·5 wt% NaCl at 303 K using electrochemical workstation (CHI instruments, 760 model). A conventional three electrode assembly having anodic-coated aluminium as working electrode, Ag/AgCl/saturated KCl as reference electrode and a platinum wire as counterelectrode was used.

3. Results and discussion

3.1 *Surface morphology*

3.1a *Influence of concentration*: To study the effect of electrolyte concentration on properties and morphology of the anodic coatings, samples were first prepared by varying the electrolyte concentration from 10 to 40 g/L with the applied current density of 0·02 A/cm^2. The anodic coating thickness obtained at various concentrations of the electrolyte is measured and the result is shown in figure 1(a, b). The coating properties show a linear relationship with the PTO concentration up to 30 g/L and later it decreases.

Figure 2 shows the surface topology of the coatings formed at various concentrations of PTO. The coating formed at a lower concentration (10 g/L) has an irregular growth of grains that are arranged at random locations as shown in figure 2(a). The coating was formed only on localized areas on the surface and most of the alloy surface is still exposed. The thickness of the coating obtained at this concentration is very low. Figure 2(b) shows that the coating formed from 20 g/L concentration of PTO has a porous structure with diameter of about 70 nm and some pores are interconnected. Usually, pore growth occurs due to the inward movement of the oxide layer at the pore bottom (barrier layer). The coating thickness increases at this concentration and some large pits are seen randomly on the surface of the coating. When the concentration was increased to 30 g/L, the coating had the same nanoarchitectures similar to those obtained in the earlier case but with a network-like porous structure with better pore ordering. While increasing the PTO concentration from 20 to 30 g/L, the pore density decreases and the pore diameter decreases from 70 to 50 nm and the interpore distance increases. Some square-shaped particles of different sizes are seen above the porous layer. The ceramic coating formed at this concentration shows maximum thickness (45·06 μm), growth rate (1 μm/min) and coating ratio (1·92). At high concentration of PTO (40 g/L) some micro cracks appear on the coating, as shown in figure 2(d). This might be the result of internal stress arising in the coating near asperities on the Al surface due to volume expansion. So the coating thickness decreases at this concentration. The best morphology of ceramic coating was obtained from

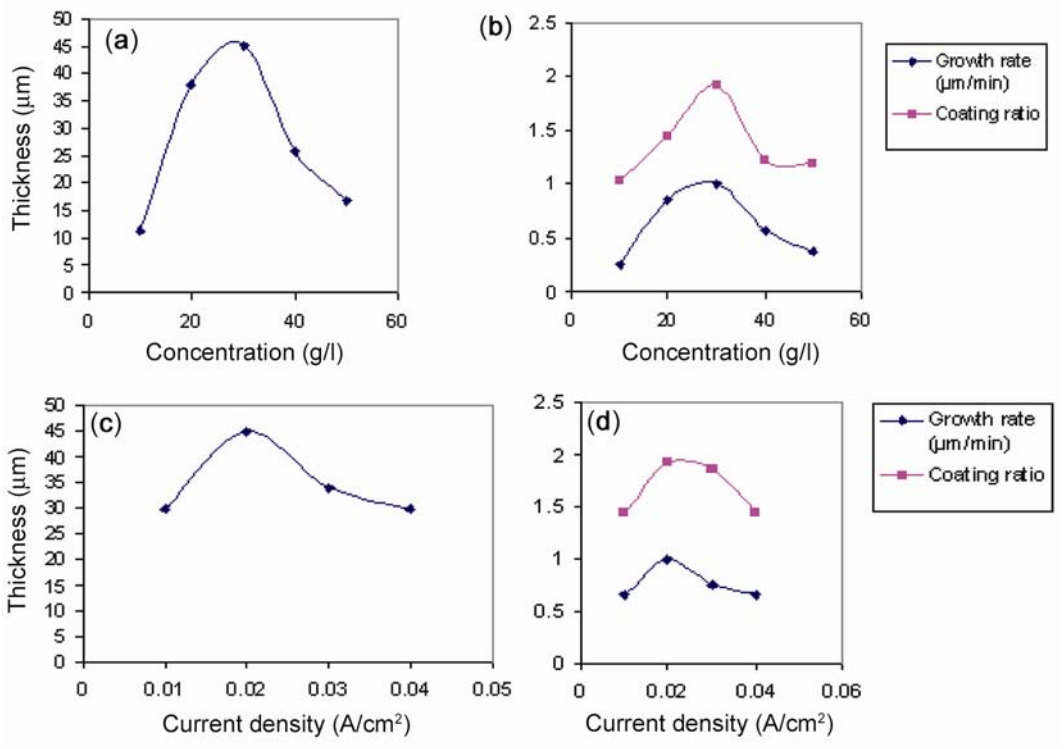

Figure 1. Effect of (i) concentration (**a**, **b**) and (ii) current density (**c**, **d**) on thickness, growth rate and coating ratio of the ceramic coating.

this series of experiments in an electrolyte solution containing 30 g/L PTO.

3.1b *Influence of current density*: The second parameter of interest investigated was current density. In order to find the ultimate condition for synthesis of ceramic coating, the effect of applied current density was studied while keeping the concentration of PTO constant. In this series of experiments, the anodization was carried out using 30 g/L concentration of PTO for 45 min and the applied current density was varied between 0·01 and 0·04 A/cm^2. Figure 1(c, d) shows that the coating properties go linearly with the current density up to 0·02 A/cm^2 and, after that, it decreases.

Figure 2(c–e) shows the surface morphology of the coatings obtained at various current densities. At lower current density (0·01 A/cm^2), small pits are formed on the surface. This is due to the localized dissolution of the previously formed oxide layer (figure 2e). The coating obtained at this condition is also very thin. At this stage, the oxidation and the field-assisted dissolution is slow, resulting in a slow inward movement of the metal oxide boundary. On increasing the current density to 0·02 A/cm^2, regularly arranged pores are formed on the surface (figure 2c). This was discussed elaborately in the earlier §3.2a. When the current density increases, initially formed small pits are converted into pores and the exposure of the aluminium to the electric field increases. So, the coating formed at this current density has less impurities, fewer defects, high micro hardness and more resistance to chemical dissolution, leading to the much better organization and uniformity of pores. At high current density (0·03 A/cm^2), the electric field and ionic current concentrated in the pores result in greater dissolution. The porous morphology, therefore, gets distorted as shown in figure 2(f). Here, the electric field dissolution of the oxide layer predominates the electrochemical formation. Based on the these SEM results, it can be concluded that the optimum conditions for getting ceramic coating with best morphology are 30 g/L concentration of PTO and 0·02 A/cm^2 current density.

3.2 *Energy dispersive X-ray spectroscopy*

Figure 3(a) represents the EDX spectrum of the ceramic coating obtained at optimized conditions. The spectra show some well-defined peaks for Al, O and Ti at 1·486, 0·525 and 4·508 KeV, respectively. Their presence proves that the coatings are mainly composed of alumina and titania. This is also evident from X-ray diffraction studies.

3.3 *X-ray diffraction study*

The XRD pattern (figure 3b) of the ceramic coatings annealed at 550 °C shows sharp and strong peaks at 44° corresponds to γ-alumina with the crystal lattice cubic/

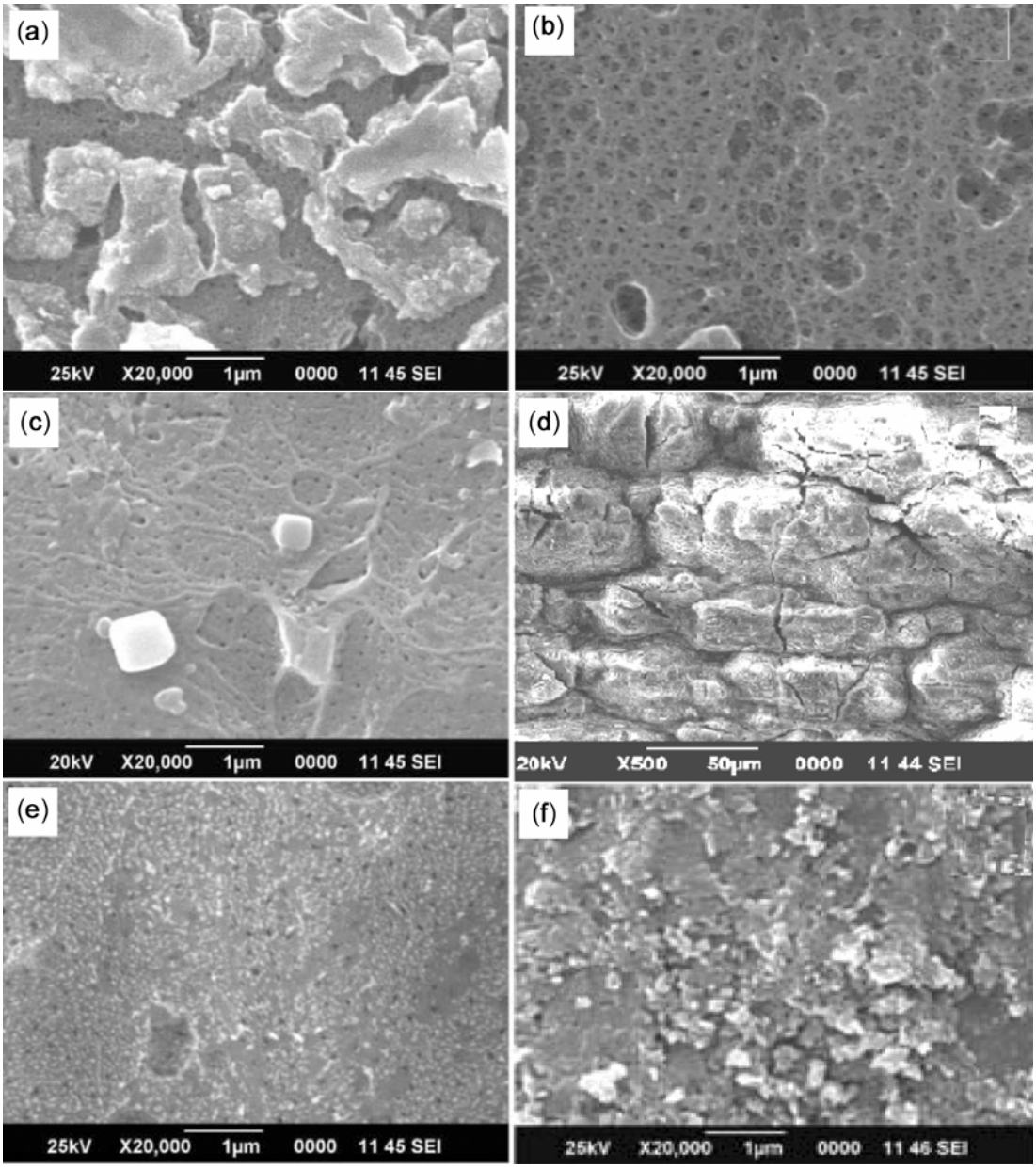

Figure 2. Scanning electron micrographs of the nanoceramic coatings: (i) various concentrations (**a**) 10, (**b**) 20, (**c**) 30, (**d**) 40 g/L and obtained at constant density of 0·02 A/cm^2 and (ii) current densities (**e**) 0·01, 0·02 (shown in (**c**)) and (**f**) 0·03 A/cm^2 obtained at constant concentration of 30 g/L.

primitive (JCPDS card: 04-0880) and the peaks at 65°, 78° correspond to titania-rutile with the crystal lattice tetragonal/primitive and rhombohedral/rhombocentered, respectively. The sharp peaks indicate the nanocrystalline nature of the coatings. The peaks show that the change in the concentration and the current density does not change the phase of the coating. The temperature 550 °C is significantly lower than that for the complete transformation of anatase-to-rutile in the case of pure TiO_2. The presence of Al_2O_3 lowers the temperature needed for the phase transformation of anatase-to-rutile TiO_2 (Gouma and Mills 2001). Further, the incorporation of TiO_2 into Al_2O_3 can accelerate the phase transformation of α-alumina to γ-alumina (Borkar and Dharwadkar 2004).

The average crystalline size of the anodic coating, obtained from various concentrations of PTO electrolyte, ranges from 104·75 to 161·47 nm and 124·06 to 154·60 nm for various current densities.

3.4 *Evaluation of corrosion resistance of ceramic coatings*

The degree of corrosion protection offered by the ceramic coating fabricated on aluminium surface by anodization

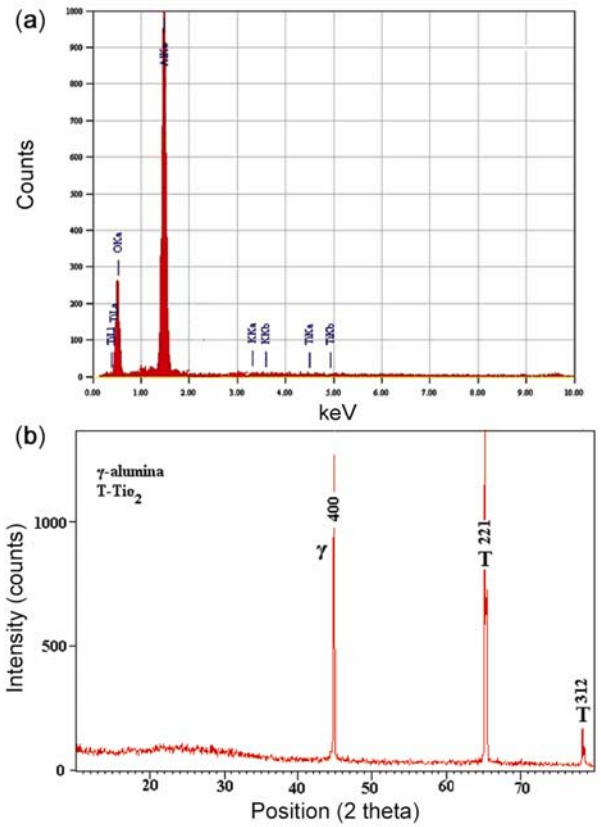

Figure 3. (**a**) Energy dispersive X-ray spectra and (**b**) X-ray diffraction pattern of ceramic coating obtained at optimized conditions.

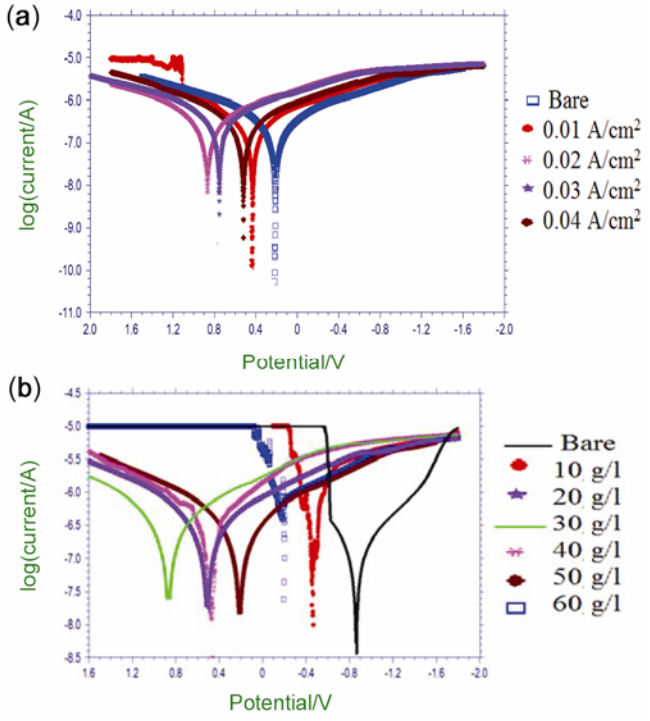

Figure 4. Comparative Tafel plots for ceramic coatings obtained at various (**a**) current densities and (**b**) concentrations along with bare aluminium.

has been investigated, using tafel polarization technique and electrochemical impedance spectroscopy.

3.4a *Tafel polarization study*: Figure 4(a, b) shows the anodic polarization behaviour of the ceramic coatings formed at various current densities and concentrations of PTO electrolyte, along with bare aluminium in 3% NaCl. The parameters obtained by fitting the potentiodynamic curves are displayed in tables 1 and 2. This technique allows quick determination and characterization of the specimen to check its passivity in the test solution. Both the current density and electrolyte concentration have an obvious influence on the corrosion resistance of anodic coating.

The results presented in figure 4(a, b) reveal that these anodized aluminium electrodes have fairly low corrosion rates and that they have better resistance to seawater corrosion compared to bare aluminium. The corrosion resistance of anodized aluminium electrode was 100 times higher than that of the bare aluminium. The ceramic coatings formed on the aluminium specimen at lower concentration of PTO and current density exhibited high corrosion current, least polarization resistance and corrosion potential.

The corrosion potential of the coatings formed on the aluminium shifted towards positive direction and *vice versa* for corrosion current when the concentration of PTO and current density increases up to 30 g/L and 0·02 A/cm^2 and above those conditions reverse trend takes place. The rationale underlying is that the coating thickness increases linearly with the PTO electrolyte concentration and the current density up to 30 g/L and 0·02 A/cm^2. So the anodized aluminium electrode is more passive against corrosion and the breakdown of this passive layer takes place at more positive potential (0·866 V). The presence of the corrosion resistance phase, titania along with alumina, is advantageous in improving the corrosion resistance of aluminium under Cl^- environment. When the current density and concentration were increased above the optimized conditions, the thickness as well as the stability of the coating decreased and some cracks also appeared in the coating. This would produce a more active centre that facilitates oxygen diffusion to the alloy surface, thereby creating a higher concentration of corrosion cells (Melchers 2001). This activates various chemical reactions, leading to pit initiation and propagation (Szklarska-Smialowska 1986). Therefore, the corrosion potential is shifted in the negative direction and the corrosion current increases. Due to the greater thickness of the coating formed at 30 g/L of PTO at 0·02 A/cm^2, it has more noble potential (0·866 V) and lowest corrosion current ($6{\cdot}285 \times 10^{-9}$ μA), corrosion rate ($8{\cdot}0951 \times 10^{-12}$ mpy) and higher polarization resistance (722532·8 Ω) compared to the coating formed at other anodization conditions.

Table 1. Corrosion parameters obtained from Tafel polarization for ceramic coatings formed in various current densities at 30 g/L concentration of PTO for 45 min at room temperature.

Current densities (A/cm^2)	Corrosion potential (V)	Corrosion current (μA)	Corrosion rate (mpy)	Polarization resistance (Ω)
Bare	–0·863	$8{\cdot}410 \times 10^{-6}$	$10{\cdot}8321 \times 10^{-9}$	8830
0·01	0·213	$7{\cdot}631 \times 10^{-7}$	$9{\cdot}8287 \times 10^{-9}$	515047·4
0·02	0·866	$6{\cdot}285 \times 10^{-9}$	$8{\cdot}0951 \times 10^{-12}$	722532·8
0·03	0·521	$7{\cdot}631 \times 10^{-8}$	$9{\cdot}8287 \times 10^{-11}$	602058·8
0·04	0·429	$7{\cdot}969 \times 10^{-8}$	$10{\cdot}2641 \times 10^{-11}$	584073·4

Table 2. Corrosion parameters obtained from Tafel polarization for ceramic coatings formed in various concentrations of PTO at current density of 0·02 A/cm^2 for 45 min at room temperature.

Various concentrations of PTO (g/L)	Corrosion potential (V)	Corrosion current (μA)	Corrosion current (mpy)	Polarization resistance (Ω)
Bare	–0·863	$8{\cdot}410 \times 10^{-6}$	$10{\cdot}8321 \times 10^{-9}$	8830
10	–0·4654	$1{\cdot}130 \times 10^{-6}$	$1{\cdot}4554 \times 10^{-9}$	99361·8
20	–0·2032	$1{\cdot}318 \times 10^{-7}$	$1{\cdot}6975 \times 10^{-10}$	274025
30	0·866	$6{\cdot}285 \times 10^{-9}$	$8{\cdot}0951 \times 10^{-11}$	722532·8
40	0·511	$6{\cdot}503 \times 10^{-8}$	$8{\cdot}3759 \times 10^{-11}$	602058·8
50	0·452	$7{\cdot}863 \times 10^{-8}$	$10{\cdot}1275 \times 10^{-11}$	556855·6
60	0·2121	$3{\cdot}867 \times 10^{-8}$	$4{\cdot}9807 \times 10^{-11}$	535396·6

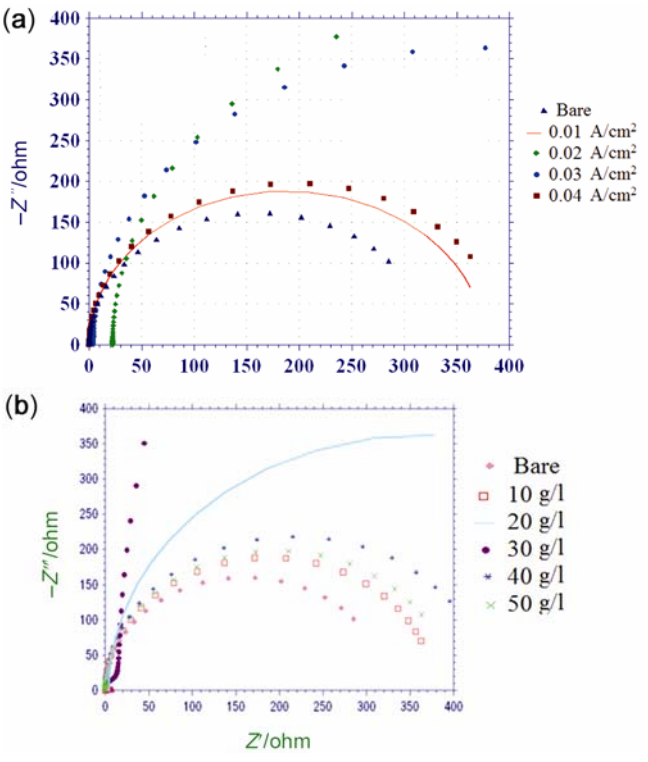

Figure 5. Comparative Nyquist impedance plots for ceramic coatings obtained at various (**a**) current densities and (**b**) concentrations along with bare aluminium.

3.4b *Electrochemical impedance spectroscopic study*: EIS enables us to determine different parameters of equivalent electrochemical systems (capacitance, resistance, etc.). Moreover, Kendig *et al* (1986) suggested that the EIS spectra obtained over a wide range of frequencies indicated that the technique was the right choice, since it was applicable for evaluating complicated corrosion processes.

The EIS characteristics of aluminium with and without anodic films in 3·5% NaCl solution were examined at open circuit potential. Figure 5(a, b) represents comparative Nyquist impedance plots of bare aluminium and anodic coatings formed on aluminium at various current densities and concentrations of PTO in 3·5% NaCl.

Based on these experimental results, electrochemical equivalent circuit was proposed to explain the experimental data of EIS, as shown in figure 6. It is a simplified electrochemical model which has been consistently reported in the references (Feng *et al* 2012; Huang *et al* 2012). As seen from the equivalent circuit, R_{sol} refers to the resistance of the solution. CPE is the electric double-layer capacitance. R_{ct} is the charge transfer resistance that represents the electrochemical corrosion rate. The larger the R_{ct}, the smaller will be the corrosion rate.

Based on the proposed equivalent circuit model these EIS curves were the best fitted. The relevant electrochemical parameters calculated from the Nyquist impedance plots are listed in the tables 3 and 4. From the figures and tables, it can be seen that the anodized electrode shows superior resistance compared to the bare aluminium due to the passivation of the electrode by the anodization. As the concentration of PTO and current density increases, the R_{ct} value increases and C_{dl} value decreases up to 30 g/L PTO and 0·02 A/cm^2 current density. Above those conditions, the values shift in the reverse direction. The reason is the same as explained in the case of tafel polarization studies. The coating formed from 30 g/L

Table 3. Influence of current density on corrosion parameters obtained from EIS curves for ceramic coatings formed from 30 g/L concentration of PTO at room temperature for 45 min.

Various current densities (A/cm^2)	R_{sol}	C_{dl} (μF cm^{-2})	R_{ct} (Ω cm^2)
Bare	$1{\cdot}3692 \times 10^{-2}$	0·0014	321·5
0·01	$1{\cdot}2055 \times 10^{-4}$	$4{\cdot}329 \times 10^{-2}$	376·3
0·02	$1{\cdot}4631 \times 10^{-7}$	$4{\cdot}439 \times 10^{-8}$	2161
0·03	$6{\cdot}4038 \times 10^{-5}$	$3{\cdot}130 \times 10^{-5}$	880·9
0·04	$4{\cdot}1733 \times 10^{-5}$	$9{\cdot}852 \times 10^{-5}$	726·2

Table 4. Corrosion parameters obtained from EIS curves for anodic coatings formed in various concentrations of PTO applying 0·02 A/cm^2 at room temperature for 45 min.

Various concentrations of PTO (g/l)	R_{sol}	C_{dl} (μF cm^{-2})	R_{ct} (Ω cm^2)
Bare	$1{\cdot}3692 \times 10^{-2}$	0·0014	321·5
10	$0{\cdot}0747 \times 10^{-3}$	$6{\cdot}784 \times 10^{-2}$	376·3
20	$0{\cdot}0164 \times 10^{-5}$	$7{\cdot}978 \times 10^{-5}$	726·2
30	$1{\cdot}4639 \times 10^{-7}$	$4{\cdot}439 \times 10^{-8}$	2161
40	$0{\cdot}0674 \times 10^{-4}$	$3{\cdot}130 \times 10^{-4}$	435·5
50	$1{\cdot}2307 \times 10^{-4}$	$9{\cdot}852 \times 10^{-4}$	394·8

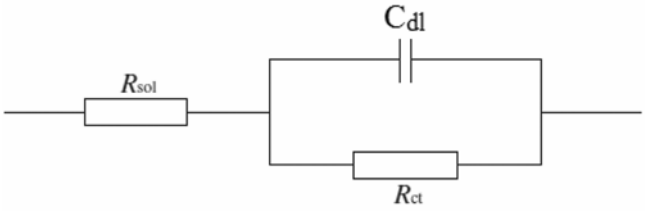

Figure 6. Equivalent circuit for the anodized aluminium.

concentration of PTO at 0·02 A/cm^2 current density has high R_{ct} value (2161 Ω cm^2) and a low C_{dl} ($4{\cdot}439 \times 10^{-8}$ μF cm^{-2}) value compared to coatings formed under other anodization conditions due to its maximum thickness. The EIS data are in good agreement with tafel studies. Based on the tafel and impedence data, 30 g/L concentration of PTO and 0·02 A/cm^2 current density were selected as the most suitable conditions to anodize Al in PTO electrolyte.

3.5 *Formation mechanism of nanoceramic coatings*

Our results demonstrate the ability to grow mixed alumina-titania oxide films that are several micrometers thick. Increasing the PTO concentration from 10 to 30 g/L leads to the increase in thickness, growth rate and coating ratio of the ceramic coatings, and above 30 g/L, the reverse takes place. In general, high electrolyte concentration increases the electric current densities in the solution and, for this reason, high concentrations of electrolyte should increase the electrode reaction rate. So, it was believed that the increase in the coating thickness was perhaps due to the increase in the reaction rate of Al^{3+} ions that were

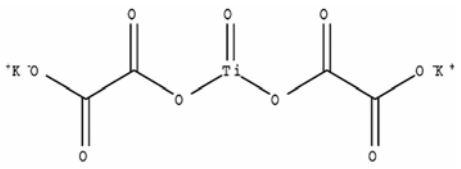

Dipotassium titanium oxide dioxalate [$K_2TiO{\cdot}(C_2O_4)_2$] noted

$$Al \rightarrow Al^{3+} + 3e^-, \quad (1)$$

$$K_2(TiO)(C_2O_4)_2 + 4H_2O \rightarrow O^{2-} + 2K^+ + [Ti(OH)_4] + 4CO_2 + 2H_2, \quad (2)$$

$$K_2(TiO)(C_2O_4)_2 + 4H_2O \rightarrow O^{2-} + 2KOH + [Ti(OH)_2]^{2+} + 4CO_2 + 2H_2, \quad (3)$$

$$2Al^{3+} + 3O^{2-} \rightarrow Al_2O_3, \quad (4)$$

$$Ti(OH)_4 \rightarrow TiO_2 + 2H_2O, \quad (5)$$

$$[Ti(OH)_2]^{2+} \rightarrow TiO_2 + H_2, \quad (6)$$

$$Al_2O_3 + TiO_2 \rightarrow \underset{\text{Alumina–titania ceramic coating}}{Al_2O_3–TiO_2}, \quad (7)$$

$$K_2(TiO)(C_2O_4)_2 \rightarrow 2K^+ + TiO_2 + CO_3^{2-} + 3CO_2 + H_2O + 2H_2, \quad (8)$$

$$2K^+ + CO_3^{2-} \rightarrow K_2CO_3, \quad (9)$$

$$2Al^{3+} + 3CO_3^{2-} \rightarrow Al_2(CO_3)_3. \quad (10)$$

Scheme 1. Proposed mechanism for the formation of Al_2O_3–TiO_2 nanoceramic coatings.

outward drifted from the aluminium specimen with oxygen and hydroxide ions supplied by the electrolyte (1–4, 7). Another probability is that the increment in PTO concentration might produce more amount of TiO_2 so that the incorporation of TiO_2 into the anodic coating increases

(5–7). EDX and XRD data also support the occurrence of TiO_2 in the anodic coating. These reasons are responsible for the formation of thick, hard and adhesive oxide films with excellent corrosion resistance in spite of its porous morphology (Guo-Hua Lv *et al* 2009; Raj *et al* 2009; Lei Wen *et al* 2010; Wanga *et al* 2013). At a very high concentration above 30 g/L, drastic increase in the pH of the electrolyte induced the dissolution of the coatings due to the formation of KOH. There are some possibilities for the formation of a small amount of potassium and aluminum carbonates (8–10). The possible reactions that are involved during the formation of ceramic coatings are given in scheme 1.

When the current density was augmented from 0·01 A/cm^2, the coating properties increased up to 0·02 A/cm^2, and it decreased thereafter. At low current density (0·01 A/cm^2), the oxidation rate was slow and resulted in a small amount of coating formation on the aluminium surface. While increasing the current density, the driving force for the movement of the ionic species required for the oxide growth increased and so it accelerated the oxidation rate. As the probability of oxidation rate increased, the thickness of the coating would supposedly increase. Above 0·02 A/cm^2, the coating properties considerably decreased because of two major reasons: (a) local joule heat effect and (b) polarization of Ti–O, Al–O, Al–O–Ti bonds that enhanced the dissolution of the coatings.

4. Conclusions

Alumina-titania nanoceramic coatings were fabricated using potassium titanium oxalate electrolyte. The maximum coating properties were obtained for the coatings formed in 30 g/L PTO and 0·02 A/cm^2 current density. From the SEM analysis, it was found that the coating formed at optimized conditions had fewer pores with better pore ordering. EDX spectra showed that the coating had peaks corresponding to Al, O and Ti. XRD analysis proved that the coating was composed of γ-alumina and rutile phase of titania. From tafel and EIS studies, it can be concluded that the coatings formed at optimized conditions has more corrosion resistance compared to other coatings.

Acknowledgement

We wish to acknowledge the financial support provided for this work by INSPIRE Division, DST, Govt of India.

Electronic Supplementary Material

Supplementary material pertaining to this article is available on the Bulletin of Materials Science website (www.ias.ac.in/matersci).

References

Borkar S and Dharwadkar S 2004 *J. Therm. Anal. Calorim.* **78** 761
Curran J A and Clyne T W 2005 *Surf. Coat. Technol.* **199** 168
Deng W H, Toepke M W and Shanks B H 2003 *Adv. Funct. Mater.* **13** 61
Despic, Parkhutik V, Bokris J O M, White R E and Conway B E (eds) 1998 *Modern aspects of electrochemistry* (New York: Plenum Press) Vol 23, p 401
Diggle J W, Downie T C and Goulding C W 1969 *Chem. Rev.* **69** 365
Feng Z S, Chen J J, Zhang R and Zhao N 2012 *Ceram. Int.* **38** 3057
García-Benjume M L, Espitia-Cabrera M I and Contreras-García M E 2009 *Mater. Charact.* **60** 1482
Gouma P I and Mills M J 2001 *J. Am. Ceram. Soc.* **84** 619
Guo-Hua L V, Chen H, Gua W C, Feng W R, Li L, Niu E W, Zhang X H and Yang S Z 2009 *Curr. Appl. Phys.* **9** 324
Hoyer P, Baba N and Masuda H 1995 *Appl. Phys. Lett.* **66** 2700
Hoyer P, Nishio K and Masuda H 1996 *Thin Solid Films* **286** 88
Ibrahim D M, Mostafa A A and Khalil T 1999 *Ceram. Int.* **25** 697
Kendig M W, Allen A T, Jeanjaquet S L, Mansfeld F and Baboian R 1986 *Electrochemical Techniques* NACE 67
Liu S, Tao W, Li J, Yang Z and Liu F 2005 *Powder Technol.* **155** 187
Martin C R 1996 *Chem. Mater.* **8** 1739
Melchers R 2001 *J. Br. Corros.* **36** 201
Mubarak Ali M and Raj V 2010 *Appl. Surf. Sci.* **256** 3841
Patermarakis G S and Kytopoulos V N 2009 *Mater. Lett.* **61** 4997
Raj V and Mubarak Ali M 2009 *J. Mater. Process. Technol.* **209** 5341
Ren T Z, Yuan Z Y and Su B L 2004 *Langmuir* **20** 1531
Szklarska-Smialowska 1986 NACE 223
Takahashi, Fukuda M, Fukuda M, Fukuda H and Yoko T 2002 *J. Am. Ceram. Soc.* **85** 2998
Wang Y, Lei T, Jiang B and Guo L 2004 *Appl. Surf. Sci.* **233** 258
Wang D, Tian Z, Shen L, Liu Z and Huang Y 2009 *Surf. Coat. Technol.* **203** 1298
Huang W, Zhou C, Liu B, Wang M, Wang H and Ma N 2012 *Surf. Coat. Technol.* **206** 4988
Wernick S, Pinner R and Sheasby P G 1987 *The surface treatment of aluminium and its alloys* (Teddington, Middlesex, UK: Finishing Publications Ltd.) 5th edn, p 140.
Wen L, Wang Y, Zhou Y, Ouyang J H, Guo L and Jia D 2010 *Corr. Sci.* **52** 2687
Wanga Y M, Tiana H, Shenb X E, Wena L, Ouyanga J H, Zhoua Y, Jiaa D C and Guoa L X 2013 *Ceram. Int.* **39** 2869
Wunderlich W, Padmaja P and Warrier K G K 2004 *J. Eur. Ceram. Soc.* **24** 313
Xue W, Wang C, Deng Z, Chen R, Li Y and Zhang T 2002 *J. Phys. Condens. Matter* **14** 10947
Yuan Z Y, Ren T Z, Vantomme A and Su B L 2004 *Chem. Mater.* **16** 5096
Zhao X, Lee U, Sea S J and Lee K H 2009 *Mater. Sci. Eng. C* **29** 1156